

Thermal conductivity modeling of periodic two-dimensional nanocomposites

Ronggui Yang and Gang Chen*

Mechanical Engineering Department, Massachusetts Institute Technology, Cambridge, Massachusetts 02139, USA

(Received 22 December 2003; revised manuscript received 11 March 2004; published 27 May 2004)

In this paper, the phonon Boltzmann equation model is established to study the phonon thermal conductivity of nanocomposites with nanowires embedded in a host semiconductor material. Special attention has been paid to cell-cell interaction using periodic boundary conditions. The simulation shows that the temperature profiles in nanocomposites are very different from those in conventional composites due to ballistic phonon transport at nanoscale. Such temperature profiles cannot be captured by existing models in literature. The general approach is applied to study silicon wire/germanium matrix nanocomposites. We predict the thermal conductivity dependence on the size of the nanowires and the volumetric fraction of the constituent materials. At constant volumetric fraction the smaller the wire diameter, the smaller is the thermal conductivity of periodic two-dimensional nanocomposites. For fixed silicon wire dimension, the lower the atomic percentage of germanium, the lower the thermal conductivity of the nanocomposites. Comparison is also made with the thermal conductivity of superlattices. The results of this study can be used to direct the development of high efficiency thermoelectric materials.

DOI: 10.1103/PhysRevB.69.195316

PACS number(s): 68.65.-k, 44.10.+i, 63.22.+m

I. INTRODUCTION

The efficiency and energy density of thermoelectric devices are determined by the dimensionless thermoelectric figure of merit $ZT = S^2 \sigma T / k$, where S is the Seebeck coefficient, σ is the electrical conductivity, k is the thermal conductivity, and T is the absolute temperature.¹ Significant advances for increasing ZT have been made based on new ideas to engineer electron and phonon transport.² One particularly fruitful and exciting approach has been the use of nanostructures, so that the electron performance can be improved or maintained concurrently with a reduction of phonon thermal conductivity.³⁻⁵ Nanostructure-based materials such as $\text{Bi}_2\text{Te}_3/\text{Sb}_2\text{Te}_3$ superlattices and $\text{PbTe}/\text{PbSeTe}$ quantum dot superlattices have shown significant increases in ZT values compared to their bulk counterparts^{6,7} due to mainly reduced phonon thermal conductivity of these structures. Nanocomposites may realize a similar thermal conductivity reduction and provide a pathway to scale-up the nanoscale effects observed in superlattices to thermoelectric material in bulk form.

Most of the previous studies on thermal transport in nanostructures have focused on thin films, semiconductor superlattices, and nanowires. One key question in modeling of the thermal conductivity in nanostructures is when the wave effect, i.e., the phonon dispersion change, should be considered.^{8,9} For example, models for phonon transport in superlattices generally fall into two groups. One group (“wave models”) assumes that phonons form superlattice bands and calculates the modified phonon dispersion using lattice dynamics or other methods.¹⁰⁻¹³ The other group of models (“particle models”) assumes that the major reason for the thermal conductivity reduction is the sequential scattering of phonons at interfaces.¹⁴⁻¹⁷ In these models, phonon transport falls in the totally incoherent regime and superlattices are treated as inhomogeneous multilayer structures. Diffuse interface scattering is usually incorporated into the Boltzmann equation (BE) as boundary conditions. These models

succeeded in fitting experimental values of several superlattice systems in the thick period range. However, because the wave nature of phonons is ignored, these models fail to explain the thermal conductivity recovery in the short period limit that is observed in some superlattices. More recently, models^{9,18} and direct simulations¹⁹ combining the above two pictures have been presented. These models and simulations further confirm the importance of diffuse interface scattering for thermal conductivity reduction. The diffuse interface scattering cannot only reduce the phonon mean free path (MFP) but also destroy the coherence of phonons. Due to the loss of coherence, the phonon dispersion change in nanostructures predicted by ideal lattice dynamics approximation cannot be realized. Previous studies on the thermal conductivity of superlattices demonstrated that classical size effect models are expected to be applicable to a wide range of nanostructures. This has been further confirmed by a recent study on developing the classical size effect model for phonon transport in nanowires and superlattice nanowires.²⁰ The model, assuming gray and diffuse phonon scattering at interfaces and side walls, has successfully explained the thermal conductivity reduction effect measured from nanowires. Based on previous studies, we will apply in this work the phonon Boltzmann equation to study the classical size effect on the thermal conductivity of nanocomposites.

Another field of related research is effective thermal conductivity of composites. The effective thermal conductivity of composites in macroscale has been studied since Maxwell (for a review, see Milton²¹) and a variety of methods have been proposed to estimate physical properties of heterogeneous media. In most of these research works, the interfaces between two heteromedia are treated as nonresistive to heat flow. The interface thermal resistance, or Kapitza resistance,²² has been considered only recently. The first two theoretical analyses that included the interface thermal resistance were conducted by Hasselman and Johnson²³ and by Benvensite,²⁴ respectively. Hasselman and Johnson extended

the classical work of Maxwell and Rayleigh to derive Maxwell–Garnett-type effective medium approximation (EMA) for calculating effective thermal conductivity of simply spherical particulate and cylindrical fiber reinforced matrix composites in which interface effect and particle size effect are included. Benveniste and Miloh²⁴ developed a general framework incorporating thermal boundary resistance by averaging all pertinent variables like heat flux and intensity over the composite medium viewed as a continuum consisting of a matrix with inclusions. Every *et al.*²⁵ refined the effective medium theory and presented an asymmetric Bruggeman type EMA, corrected for Kapitza resistance, as a simple solution for high volumetric fraction of inclusion, based on Bruggeman’s integration-embedding principle. A noticeable work was by Nan *et al.*,²⁶ who adopted the multiple scattering theory²⁷ to develop a more general EMA formulation for the effective thermal conductivity of arbitrary particulate composites with interfacial thermal resistance. They considered the properties of the matrix and reinforcement, particle size and size distribution, volume fraction, interface resistance, and the effect of shape. Other models have also been proposed including the bounding model^{28,29} and thermal resistance network theory. Numerical simulation of thermal conductivity of composites can also be found in literature.^{30–33} However, these macroscopic models are developed based on Fourier heat conduction theory that is not valid at nanoscale due to the ballistic phonon transport.

So far, there are not many theoretical studies on the thermal conductivity of nanocomposites despite their importance in both thermoelectrics and thermal management of electronics (especially the development of thermal interface materials). Closely related works are done by Khitun *et al.*³⁴ and Balandin and Lazarenkova³⁵ to explain the ZT enhancement of Ge quantum dot structures (where Ge quantum dots are ~ 4 nm and can be thought of as nanoparticles). The model by Khitun *et al.* calculates the reduced thermal conductivity through the relaxation time change due to the nanoparticles embedded using the Mathiessen rule.³⁶ They used the Mie theory for acoustic wave scattering to calculate the scattering cross section of a single particle and thus the additional relaxation time due to single particle scattering. Their method is valid if there is no inelastic scattering inside the particle and the interface scattering must be specular.³⁷ This approach does not recover to bulk material properties of composites since the thermal conductivity of nanoparticle material does not get into the final picture. Similar to the wave model of superlattices, Balandin and Lazarenkova³⁵ assumed that a new homogeneous material is formed and calculates the new electron and phonon dispersion relation thus the group velocity reduction. This approach requires phonon coherence over several unit cells and does not apply to diffuse interface scattering as observed in previous studies on superlattices.

The motivation of this work is to develop a microscopic framework for thermal conductivity of nanocomposites in terms of the phonon particle transport model. For simplicity, we will study the thermal conductivity of periodic two-dimensional (2D) nanocomposites. The model will help to understand some basic physical phenomena that exist in

nanocomposites and serve as a prototype to be further developed to characterize more complex nanocomposites, such as nanoparticle composites. Some fundamental questions, such as (a) how is phonon transport in nanocomposites different from that in macroscale composites, (b) what is the behavior of the size effect in nanowire-embedded composites, and (c) can nanocomposites have lower effective thermal conductivity than a superlattice, will be addressed in the investigation.

II. THEORETICAL MODEL

Based on the reasoning that the phonon particle model can be a good predictive tool for thermal conductivity of nanocomposites, we focus our work on the phonon transport in nanowire-embedded composites for the case where the heat-flow direction is perpendicular to the wire axis. As shown in Fig. 1(a), there is no heat flow along the wire axis thus the problem is simplified to two-dimensional although the nature of phonon transport is three-dimensional in nature as shown in Fig. 1(c). The unit cell to be simulated is shown in Fig. 1(b). The detail about the interface and boundary condition will be presented in a later section. To make a comparison, we also calculated the cross-plane thermal conductivity of a simple one-dimensional Si–Ge layered structure, which is often called superlattices when the thickness of each layer is tens of nanometers, as shown in Fig. 1(d). To establish the phonon particle model the following assumptions are made: (1) the phonon wave effect can be excluded; (2) the frequency-dependent scattering rate in the bulk medium is approximate by an average phonon MFP; and (3) the interface scattering is diffuse.

A. Phonon Boltzmann equation

With the above assumptions, the phonon BE can be expressed in terms of the total phonon intensity defined as^{38,39}

$$I_i = \frac{1}{4\pi} \sum_m \int_0^{\omega_{\max}} |v_{mi}| f \hbar \omega D_{mi}(\omega) d\omega, \quad (1)$$

where subscript i ($=1,2$) denotes properties of the host and wire material (or alternative material of a 1D layered structure, in this work $i=1$ is for germanium and $i=2$ for silicon), $D(\omega)$ is the density of states per unit volume, f the phonon distribution function, \hbar the Planck constant, $|v_{mi}|$ the magnitude of the phonon group velocity, ω the phonon frequency, and ω_{\max} is the maximum frequency of each polarization. The summation index m is over the three phonon polarizations. The purpose of introducing the phonon intensity concept³⁸ is for the mathematical convenience because the concept of photon intensity is widely used in thermal radiation literature and many results in radiative transfer might be used for phonon transport studies.^{40,41}

The 2D phonon BE under the single mode relaxation time approximation can be written as

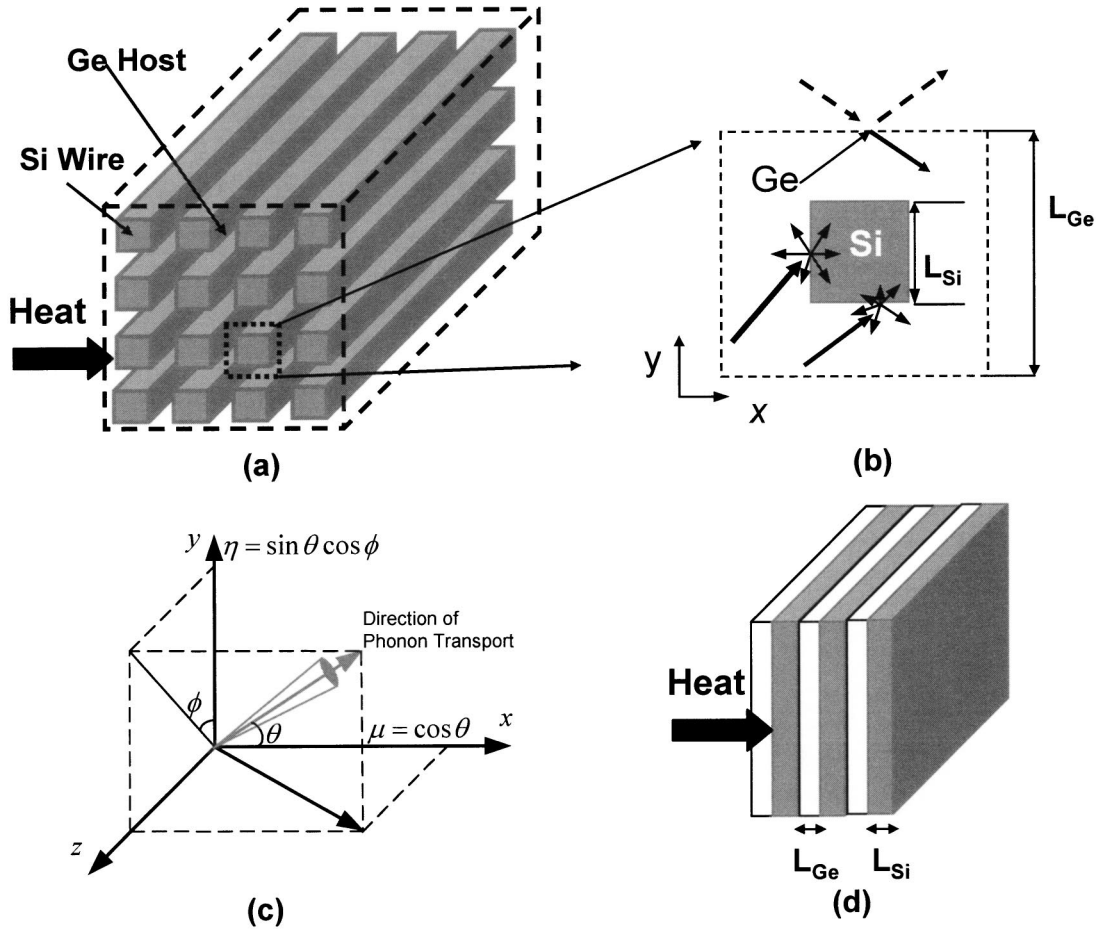


FIG. 1. (a) Heat flow across periodic 2D composite with silicon wires embedded in germanium host, (b) the unit cell to be simulated, (c) local coordinate used in phonon Boltzmann equation simulation, and (d) heat flow across 1D Si-Ge layered structure (superlattice).

$$\sin \theta_i \cos \phi_i \frac{\partial I_i}{\partial y} + \cos \theta_i \frac{\partial I_i}{\partial x} = -\frac{I_i - I_{oi}}{\Lambda_i}, \quad (2)$$

where θ and ϕ , as shown in Fig. 1(c), are the polar and the azimuthal angles, respectively, and Λ is the average phonon MFP. I_{oi} is determined by the Bose-Einstein distribution of phonons and depends on the local equilibrium temperature. In nanostructures, however, local equilibrium cannot be established and thus the temperature obtained should not be treated the same as the case of local thermal equilibrium. An energy balance shows that I_{oi} can be calculated from^{16,42}

$$\begin{aligned} I_{oi}(x, y) &= \frac{1}{4\pi} \int_{4\pi} I_i(\mathbf{r}, \mathbf{\Omega}) d\Omega \\ &= \frac{1}{4\pi} \int_0^{2\pi} \int_0^\pi I_i(x, y, \theta, \phi) \sin \theta d\theta d\phi \end{aligned} \quad (3)$$

and the corresponding temperature obtained is a measure of the local energy density. We note the equations for the 1D layered structure are much simpler because the intensity does not depend on the ϕ direction and y position.

A rigorous phonon transport simulation should incorporate the frequency dependence of phonon relaxation time and

group velocity, and thus account for interactions among phonons of different frequencies. This will relax the assumption (2). However, it requires solution of the phonon BE for many different frequencies. Previous works show that an average MFP is a good approximation for thermal conductivity modeling across the interfaces (cross-plane transport).¹⁶ For transport parallel to the interface, frequency dependent relaxation time gives a better solution.¹⁴ However, the existing theories for the frequency dependence of relaxation time contain large uncertainties because they are based on many approximations and rely on the fitting parameters from experimental data.⁴³ Therefore we will use a frequency independent phonon MFP for simplicity. Often the phonon MFP Λ is estimated from the thermal conductivity, the specific heat, and the speed of sound, according to the standard kinetic theory expression,

$$k = \frac{1}{3} C v \Lambda, \quad (4)$$

where C is the volumetric specific heat. This method, however, neglects the facts that at room temperature most acoustic phonons are populated close to the zone boundary where the phonon group velocity is significantly smaller than the sound velocity and that the optical phonons contribute a significant portion of specific heat but little to thermal conduc-

TABLE I. Room-temperature parameters used in the calculation.

	C (J/m ³ K)	v (m/s)	k (W/m K)	a (nm)
Silicon	0.93×10^6	1804	150	0.5431
Germanium	0.87×10^6	1042	60	0.5658

tivity due to their near zero group velocity. A better estimation of the phonon MFP and the group velocity can be obtained by approximating the dispersion of the transverse and the longitudinal-acoustic phonons with simple sine functions and subtracting the optical phonon contribution to the specific heat C in calculating the phonon MFP. This estimation leads to a mean free path in silicon of the order of 250–300 nm at room temperature. Experiments and modeling from Goodson's group also lead to similar numbers.⁴⁴ The method gave a better fitting of the experimental thermal conductivity data on superlattices than that based on bulk specific heat for C and the speed of sound for v in Eq. (4).^{14,16} In our analysis, some parameters used are taken from Ref. 16 as listed in Table I.

B. Boundary and interface conditions

Mathematically, the structure of the BE demands the boundary conditions to be specified on those parts of boundaries where the characteristics point into the domain.⁴⁵ This boundary condition is termed as emitted temperature at wall.¹⁶ Most of the previous works on phonon transport simulation used a specified emitted temperature boundary condition. This can give an artificial temperature jump at the boundaries due to the additional nonphysical scattering at the boundaries.⁴⁶ A more physical boundary condition is desirable to simulate phonon transport in realistic structures. In this work, the periodic boundary condition is used based on the underlying physics for phonon transport in periodic structures. As shown in Fig. 1(b), heat is enforced to flow in the x direction. The specular reflected boundary conditions are enforced at $y=0$ and $y=L_{\text{Ge}}$ boundaries due to symmetry,

$$I(x, L_{\text{Ge}}, \theta, \phi) = I(x, L_{\text{Ge}}, \theta, -\phi), \quad (5)$$

$$I(x, 0, \theta, \phi) = I(x, 0, \theta, -\phi). \quad (6)$$

In the x direction, we applied periodic boundary conditions. At equilibrium, the phonon distribution, i.e., the phonon intensity [see Eq. (1)], is isotropic. If heat is enforced to flow, the phonon distribution/intensity will be distorted. Physically the periodic boundary condition means that the distortion of phonon intensity in each direction at each point $(0, y)$ at the $x=0$ boundary is the same as the distortion in the corresponding direction at the corresponding point (L_{Ge}, y) at the $x=L_{\text{Ge}}$ boundary. The equation can be expressed as

$$I(L_{\text{Ge}}, y, \theta, \phi) - I_0(L_{\text{Ge}}, y) = I(0, y, \theta, \phi) - I_0(0, y). \quad (7)$$

With this boundary condition, the total surface heat flux is conserved in the x direction and the cell–cell interaction is taken into account. Because of the periodicity, the phonon

transport of the whole structure can be represented by that in the unit cell. Boundary conditions thus defined require an iterative scheme to solve the equation, which implies that it is more complicated than the front-to-end scheme that is usually adopted to solve the emitted temperature boundary condition problems. This periodic boundary condition has been used in studying the cross-plane thermal conductivity of superlattices (which is a 1D structure) before.¹⁶ It can be proven that the temperature difference across the unit cell should be independent of y . That is,

$$I_o(0, y) - I_o(L_{\text{Ge}}, y) = \frac{C_1 v_1 [T(0, y) - T(L_{\text{Ge}}, y)]}{4\pi} = \text{const.} \quad (8)$$

In our simulation, we superimposed $T(0, y) - T(L_{\text{Ge}}, y) = 1$ K in the above equation. If we do not superimpose such a temperature difference in the program, Eq. (7) will automatically converge to a constant temperature difference $T(0, y) - T(L_{\text{Ge}}, y)$ value. The converged value varies with simulated structures. But the final results of thermal conductivity value do not depend on whether the temperature difference is superimposed. However, the calculation is much faster when the temperature difference value is superimposed. We should note that superimposing the temperature difference across the unit cell is physically different from superimposing temperature (either emitted or Fourier-limit temperature) at each boundary.

The interface scattering between the nanowire and the host material is assumed to diffuse. Ziman³⁶ proposed the following expression for estimating the interface specular parameter p :

$$p = \exp\left(-\frac{16\pi^3 \delta^2}{\lambda^2}\right), \quad (9)$$

where δ is the characteristic interface roughness and λ is the characteristic phonon wavelength. At room temperature, the characteristic phonon wavelength $\lambda = hv/k_B T$ is about 1 nm, where h is the Planck constant, k_B is the Boltzmann constant, and v is the sound velocity in the material. Clearly even one monolayer roughness $\delta \sim 0.3$ nm gives an interface specular parameter $p=0$, and allows for totally diffuse interface assumption. Determining the phonon reflectivity and transmissivity at interface is difficult as in the treatment of the classical thermal boundary resistance problem.^{47–49} One rather crude model is called the diffuse mismatch model,⁴⁹ which assumes that phonons emerging from the interface do not really bear any relationship to its origin, i.e., one cannot tell which side they come from. This assumption implies that

$$T_{d21} = R_{d12} = 1 - T_{d12}, \quad (10)$$

where the second equation comes from the energy conservation identity $R_{d12} + T_{d12} = 1$. We remind again that subscript 12 means from medium 1 into medium 2 and vice versa. Dames and Chen²⁰ obtained the following equation for T_{d12} , which is expected to be valid over a wide temperature range:

$$T_{d12}(T) = \frac{U_2 v_2}{U_1(T) v_1 + U_2(T) v_2}, \quad (11)$$

where U is the volumetric internal energy.

With the given interface transmissivity and reflectivity, we can write down the phonon intensity at interfaces. As an example, the phonon intensity for $\theta > 0$ at the $x = (L_{\text{Ge}} - L_{\text{Si}})/2$, $(L_{\text{Ge}} - L_{\text{Si}})/2 \leq y \leq (L_{\text{Ge}} + L_{\text{Si}})/2$ interface can be written from the energy balance equation.

$$\begin{aligned} & \int_0^{2\pi} \int_0^{\pi/2} I\left(\frac{L_{\text{Ge}} - L_{\text{Si}}}{2}, y, \theta, \phi\right) \cos \theta \cdot \sin \theta d\theta d\phi \\ &= R_{d21} \int_0^{2\pi} \int_{\pi/2}^{\pi} I\left(\frac{L_{\text{Ge}} - L_{\text{Si}}}{2}, y, \theta, \phi\right) \cos \theta \cdot \sin \theta d\theta d\phi \\ &+ T_{d12} \int_0^{2\pi} \int_0^{\pi/2} I\left(\frac{L_{\text{Ge}} - L_{\text{Si}}}{2}, y, \theta, \phi\right) \cos \theta \cdot \sin \theta d\theta d\phi. \end{aligned} \quad (12)$$

Because the phonons are scattered diffusely at interfaces, the phonons leaving an interface are isotropically distributed, and Eq. (11) can be written as

$$\begin{aligned} I\left(\frac{L_{\text{Ge}} - L_{\text{Si}}}{2}, y, \theta, \phi\right) &= \frac{R_{d21}}{\pi} \int_0^{2\pi} \int_{\pi/2}^{\pi} I\left(\frac{L_{\text{Ge}} - L_{\text{Si}}}{2}, y, \theta, \phi\right) \\ &\times \cos \theta \cdot \sin \theta d\theta d\phi \\ &+ \frac{T_{d12}}{\pi} \int_0^{2\pi} \int_0^{\pi/2} I\left(\frac{L_{\text{Ge}} - L_{\text{Si}}}{2}, y, \theta, \phi\right) \\ &\times \cos \theta \cdot \sin \theta d\theta d\phi \quad \text{for } \theta > 0. \end{aligned} \quad (13)$$

Phonons leaving for $\theta < 0$ and other interfaces can be similarly written.

C. Method of numerical solution

Equation (2) is similar to the photon radiative transport equation (RTE).⁴² The key is to solve for the intensity distribution $I(\mathbf{r}, \mathbf{\Omega})$. Once the intensity is found by solving Eq. (2), the heat flux $q_x(x, y)$, $q_y(x, y)$ and the effective temperature $T(x, y)$ can be determined through the numerical integration over the whole solid angle 4π . A variety of solution method is available in the thermal radiative transfer literature.^{40,41} The most often used methods are the discrete ordinates method (DOM)⁵⁰ and the finite volume method.⁵¹ The discrete ordinate method is a tool to transform the equation of radiative transfer into a set of simultaneous partial differential equations. This is based on a discrete representation of directional variation of intensity. A solution to the transport problem is found by solving the equation of radiative

transfer for a set of discrete directions spanning the entire solid angle. The integrals over the solid angle are approximated by numerical quadratures. For phonon transport in nanostructures, the challenge is to reduce the ‘‘ray effect,’’ which often happens similarly in thermal radiation in the optical thin limit. In our previous work,⁴⁶ double Gauss-Legendre quadratures have been used to replace the conventional S_N quadratures for the discrete ordinate method and demonstrated to successfully resolve the ray effect problem of phonon transport simulation in nanostructures. We briefly discuss the calculation method here. The method separately discretizes the integrating points in the $\mu = \cos \theta$ (the angle θ) and the angle ϕ using Gauss-Legendre quadrature. To obtain high accuracy, μ is discretized into 120 points from -1 to 1 and ϕ is discretized into 24 points for $0 \sim \pi$ (not $0 \sim 2\pi$ due to symmetry). Then Eq. (3) can be written in discrete form as

$$I_0(x, y) = \frac{2}{4\pi} \sum_m \sum_n I(x, y, \mu_n, \phi_m) w_n w'_m. \quad (14)$$

The weights satisfy $\sum_m \sum_n w_n w'_m = 2\pi$. In order to accurately capture the physics of the transport phenomena and minimize the calculation time, a nonuniform grid system is used. The step scheme is used for spatial discretization. Total spatial grids of 102×102 are used in the calculation. Fewer points in both spatial and angular coordinates can be used for faster calculation. The equation is solved by iteration over the value of the equivalent equilibrium intensity $I_0(x, y) = 2/4\pi \sum_m \sum_n I(x, y, \mu_n, \phi_m) w_n w'_m$. When the relative error of the calculated value of the equivalent equilibrium intensity between two iteration steps is less than 2×10^{-6} , the program is assumed to converge and the effective temperature and heat flux are calculated.

Although at nanoscale, temperature cannot be defined as a measure of equilibrium, we can use the effective temperature to reflect the local energy density inside the medium.^{36,39} Assuming constant specific heat over a wide temperature range, we can write the effective temperature as

$$T(x, y) = \frac{4\pi I_0(x, y)}{C|v|} = \frac{1}{C|v|} \sum_n \sum_m I(x, y, \mu_n, \phi_m) w_n w'_m. \quad (15)$$

The heat fluxes at every point can be accordingly written as

$$q_x(x, y) = \sum_m \sum_n I(x, y, \mu_n, \phi_m) \mu_n w_n w'_m, \quad (16)$$

$$q_y(x, y) = \sum_m \sum_n I(x, y, \mu_n, \phi_m) \sqrt{1 - \mu_n^2} \cos \phi_m \cdot w_n w'_m, \quad (17)$$

where q_x and q_y are heat flux in the x and y directions, respectively. After local effective temperature distribution and heat flux are obtained, the thermal conductivity calculation is straightforward, taking advantage of the unit cell concept. The surface heat flux in the x direction can be calculated as

$$Q_x(x) = L_z \int_0^{L_{\text{Ge}}} q_x(x, y) dy, \quad (18)$$

where L_z is the unit length in the z direction. Equations (5) and (6), i.e., the specular reflected boundary conditions enforced at $y=0$ and $y=L_{\text{Ge}}$ boundaries have ensured $Q_x(x) = \text{const}$. The average energy density (average temperature) at each y - z plane along the x direction can be written as

$$\bar{T}(x) = \frac{1}{L_{\text{Ge}}} \int_0^{L_{\text{Ge}}} T(x, y) dy. \quad (19)$$

Therefore the effective thermal conductivity k of the composite can be obtained as

$$k = \frac{Q_x}{L_z [\bar{T}(L_{\text{Ge}}) - \bar{T}(0)]} \quad (20)$$

from

$$Q_x = k(L_z L_{\text{Ge}}) \frac{[\bar{T}(L_{\text{Ge}}) - \bar{T}(0)]}{L_{\text{Ge}}}. \quad (21)$$

The following dimensionless parameters have been introduced to present temperature and heat flux results:

$$q^* = \frac{q}{C_1 v_1}, \quad Q_x^* = \frac{Q_x}{L_{\text{Ge}} L_z C_1 v_1}, \quad x^* = \frac{x}{L_{\text{Ge}}}, \quad y^* = \frac{y}{L_{\text{Ge}}}. \quad (22)$$

III. RESULTS AND DISCUSSIONS

A. Nonequilibrium temperature and heat flux distribution

Figures 2(a) and 2(c) show the effective temperature distribution in the composite structures with silicon wire dimension of $L_{\text{Si}} = 268$ nm and $L_{\text{Si}} = 10$ nm, respectively. The atomic percentage is 20% for Si and 80% for Ge. Simple calculation gives the geometric ratio $L_{\text{Ge}}/L_{\text{Si}} = 2.35$. The choosing of $L_{\text{Si}} = 268$ nm is based on the fact that the MFP value is around 268 nm calculated from Eq. (4) by using the parameters listed in Table I. Figure 2(a) is very close to the temperature we expect in macroscale composites with interface thermal resistance. Therefore, for a wire dimension larger than 268 nm, the effective temperature distribution is expected to be similar to that plotted in Fig. 2(a). The comparison of Figs. 2(a) and 2(c) shows that the temperature or energy density distribution at nanoscale in periodic 2D composites can be very different from that at macroscale due to the ballistic nature of phonons. To better understand the effect of interface thermal resistance, we plot the temperature distribution along the x direction at certain fixed y positions of the two structures in Figs. 2(b) and 2(d). Apparent temperature jumps at the wire–host material interfaces are clearly shown in Figs. 2(b) and 2(d). There are also temperature jumps along the y direction as indicated in Figs. 2(a) and 2(c). The larger the wire dimension, the lower the temperature jump relative to the total temperature difference across the interface, and thus the lower the contribution

of the interface resistance to the effective thermal resistance of the composite. When the nanowire dimension is much smaller than the phonon MFP, say $L_{\text{Si}} = 10$ nm, the temperature gradient along the x direction can be negative in some local regions. The heat fluxes in the x direction, however, are always positive as shown in Figs. 3(a) and 3(b). This phenomenon was not observed before in macroscale composites and cannot be predicted by Fourier heat conduction based theories. Another question that may raise is whether the results shown in Figs. 2(c) and 2(d) violate the second law of thermodynamic because the temperature inside the cell is larger than the cell boundary. To answer this question, we should first remind, as pointed out before, that temperature as defined is not the same as the case of thermal equilibrium or local thermal equilibrium. When ballistic transport dominates, no local thermal equilibrium can be established and temperature calculated represents the local energy density. Figures 4(a) and 4(b) illustrate the mechanisms of the observation in Fig. 2. When L_{Si} is much smaller than the phonon MFP, the internal scattering in the medium (both host material and the wire) is negligible. We further assume that the phonon reflectivity is unity at the wire and host material interface. Then the scenario can be simplified as thermal radiation in vacuum with opaque wire inclusions (host material–vacuum, interface–solid wall, wire–opaque solid body). Referring to Fig. 4(a), we are interested in knowing the temperature distribution of points A – F when the heat is enforced to flow in the x direction. We can qualitatively call the left half of the region shown as the “hot” region and the right half as the “cold” region. As shown in the figure, points D and F “see” the hot region and points A and C “see” the cold region, thus points D and F locally receive higher energy phonons and have higher effective temperature than points A and C . Moving from point A to F (or from C to D), more hot area is seen than cold area, thus the effective temperature increases. Comparing to D and F , point E has a lower temperature due to a small view factor from the hot region. Similarly point B has a higher effective temperature than A and C . Figure 2 shows the temperature distribution only in one unit cell. To visualize the temperature distribution, one needs to stitch several periods of Fig. 2. Figure 4(b) shows the temperature distribution along x at several y points over three periods. The energy over those regions with even higher temperature than the unit cell boundary comes from the much higher temperature region in their previous cells. The results do not violate the second law of thermodynamics.

B. Effect of wire dimension

To calculate the effective thermal conductivity of composites, the surface heat flux and the average temperature (average energy density) at each y - z plane along the x direction is calculated. As examples, Fig. 5 shows the dimensionless average energy density distribution along the x direction in a $\text{Si}_{0.2}\text{Ge}_{0.8}$ composite with a silicon wire dimension of $L_{\text{Si}} = 268$ and 10 nm, respectively. The dimensionless surface heat flux is conserved to $Q_x^*(x) = 0.088$ for an $L_{\text{Si}} = 268$ nm composite and $Q_x^*(x) = 0.037$ for an $L_{\text{Si}} = 10$ nm composite. Again, the surface heat flux is conserved and the temperature

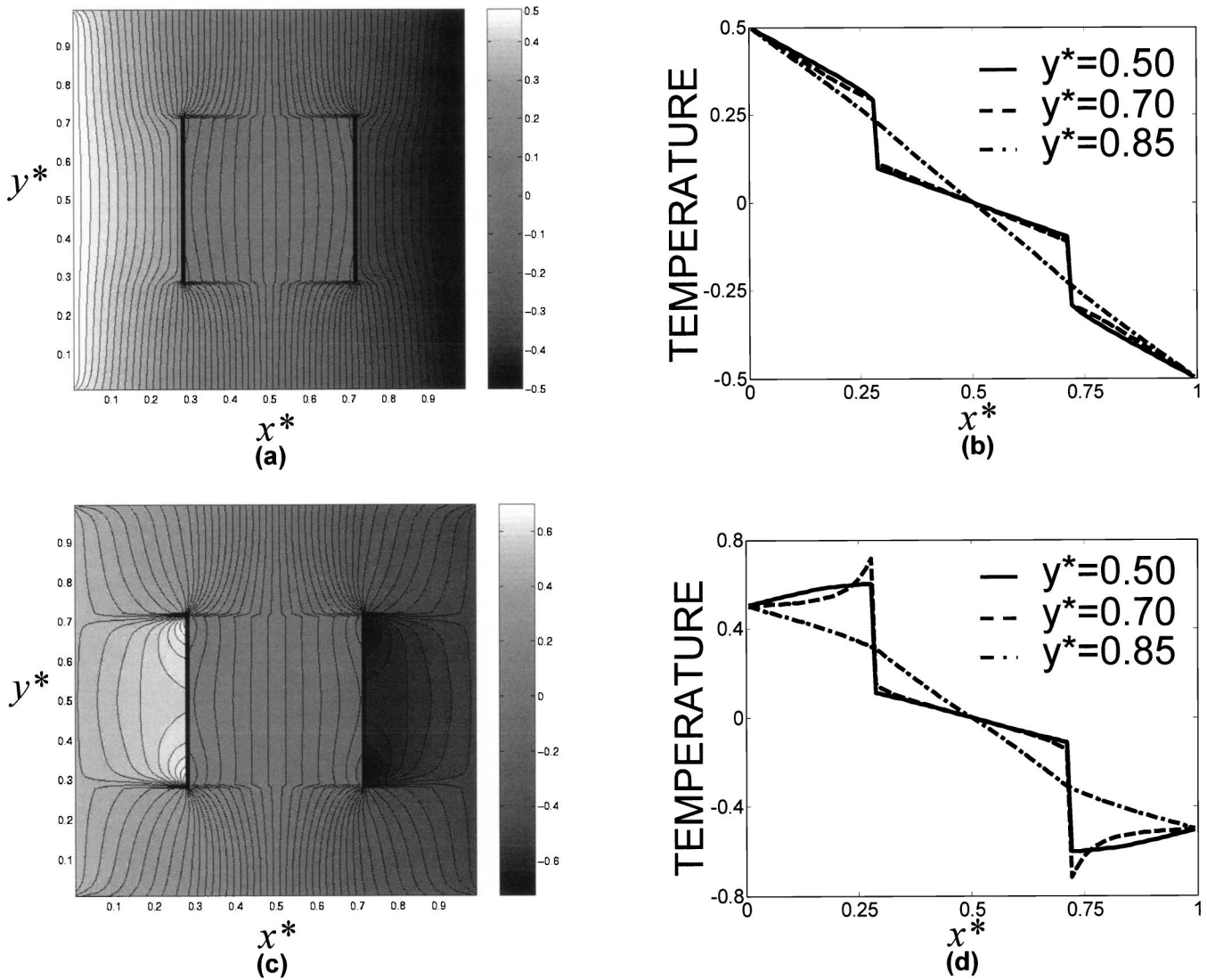


FIG. 2. Effective temperature ($T - T_{\text{ref}}$) distribution in the unit cell of $\text{Si}_{0.2}\text{-Ge}_{0.8}$ composites with $T(0,y) - T(L_{\text{Ge}},y) = 1$ K applied for different wire dimensions: (a) temperature contour for $L_{\text{Si}} = 268$ nm, (b) the temperature distribution along x^* at $y^* = 0.5, 0.7,$ and 0.85 for $L_{\text{Si}} = 268$ nm, (c) temperature contour for $L_{\text{Si}} = 10$ nm, and (d) the temperature distribution along x^* at $y^* = 0.5, 0.7,$ and 0.85 for $L_{\text{Si}} = 10$ nm. The temperature discontinuity at the interface is clearly shown. The temperature distribution in $L_{\text{Si}} = 10$ nm nanocomposite is very different from macroscale composites due to the ballistic phonon transport at nanoscale and cannot be captured by Fourier heat conduction theory.

jump appears at the interface. The smaller the wire dimension, the larger the average temperature jump and thus the larger is the interface resistance contribution to the effective thermal resistance of the composite. We can expect that when the wire dimension is 2 to 3 times or even larger than the silicon MFP, the contribution of the interface thermal resistance will be negligible and the results will recover the Fourier limit. Figure 6 shows the thermal conductivity of $\text{Si}_{0.2}\text{-Ge}_{0.8}$ composites as a function of the silicon wire dimension. To make a comparison, we include the results of cross-plane (perpendicular to the interfaces) thermal conductivity of a simple one-dimensional Si-Ge layered structure (superlattices). Simple calculation shows that the thickness of the germanium layer should be 4.52 times the thickness of the silicon layer in 1D stacks with a germanium atomic percentage of 80%. Figure 6 clearly

shows that at constant volumetric fraction (or atomic percentage) the smaller the characteristic length of silicon (the silicon wire dimension in composites and the thickness of the silicon layer in superlattices), the smaller the thermal conductivity. The simple 1D layered structure has a lower thermal conductivity than periodic nanowire composites at this atomic percentage. We point out that the thermal conductivity of superlattices calculated here is lower than the experimental data because the interface scattering in superlattices may not fall into a totally diffuse scattering limit.^{14,16} The comparison shown in this paper is just for theoretical consistency.

C. Effect of atomic percentage

Some other questions of interests are: (1) can the thermal conductivity of nanowire composites be lower than that of

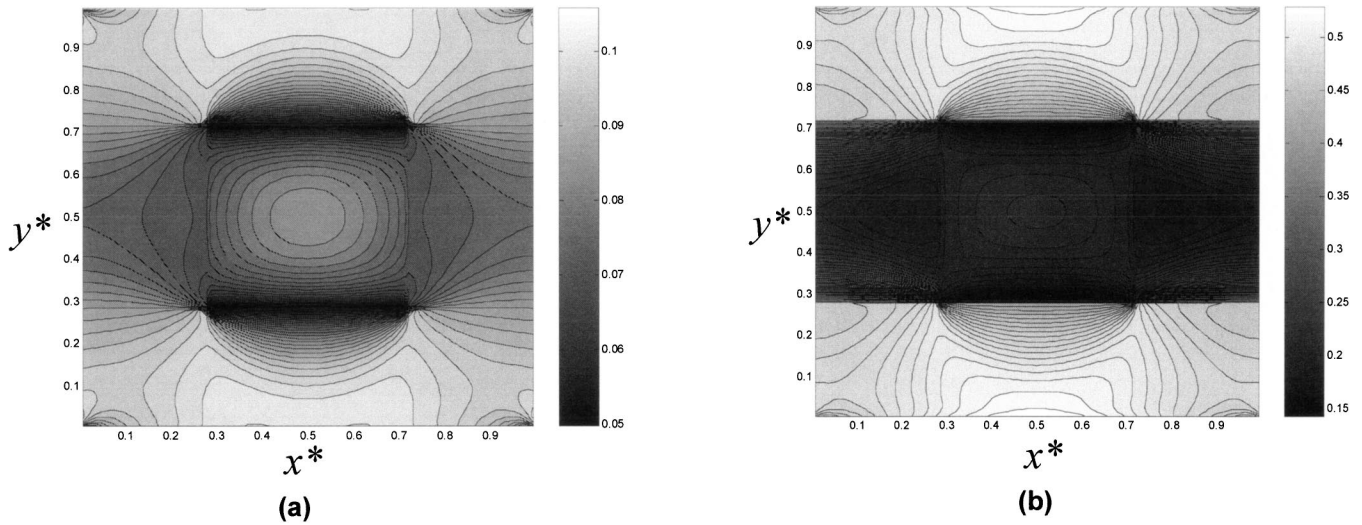


FIG. 3. The dimensionless heat flux distribution in the x direction q_x^* : (a) $L_{Si}=268$ nm composite, and (b) $L_{Si}=10$ nm composite. It shows that the x -directional heat flux is always positive even in the localized negative temperature gradient region shown in Fig. 2.

simple 1D stacks (superlattice)? (2) How the thermal conductivity changes with the atomic percentage? Figure 7 shows the thermal conductivity of $Si_{1-x}Ge_x$ composites as a function of atomic percentage x of germanium for wire dimensions L_{Si} of 50 and 10 nm, respectively. By changing the atomic percentage, the geometric ratio of the unit cell, i.e., the dimension of germanium, is changed in the numerical simulation. It shows that for a fixed silicon wire dimension, the lower the atomic percentage of germanium; the lower is the thermal conductivity of the nanocomposites. This is very different from macroscale composites and nanoparticle-filled polymers, in which thermal conductivity of the composites increases with the decreasing volumetric fraction of the low thermal conductivity component. This is caused by the ballistic transport of phonons in both the host material and the nanowires, and the interface resistance between the host material and the nanowires. In polymer nanocomposites, the thermal conductivity of the host polymer is usually very low and the thermal transport in polymers is diffusive. Thus the thermal conductivity of polymer nanocomposites increases with the volumetric fraction of high thermal conductivity nanoparticle fillers. Figure 7 also shows that the thermal conductivity of the periodic 2D nanocomposites is lower than that of the superlattice with corresponding characteristic length when the atomic percentage x of germanium is lower than 35%. Simple calculation shows that the geometric ratio L_{Ge}/L_{Si} is around 1.182 when $x=0.35$. For a simple 1D layered structure as shown in Fig. 8(a), phonons experience cross-plane interface scattering in all the cross-sectional area z - y when the heat is enforced to flow in the x direction. Comparing Figs. 8(a) and 8(b), we know that phonons can flow through a fraction of $(L_{Ge} - L_{Si})/L_{Ge}$ open area without experiencing cross-plane interface scattering in nanocomposites. However, phonons must experience an additional fraction of L_{Si}/L_{Ge} interface scattering parallel to the heat flow direction (in-plane scattering). When the thermal conductivity of a simple 1D layered structure is the same as that of the periodic 2D nanocomposites at $x=0.35$, we can approximately infer that a fraction of L_{Si}/L_{Ge}

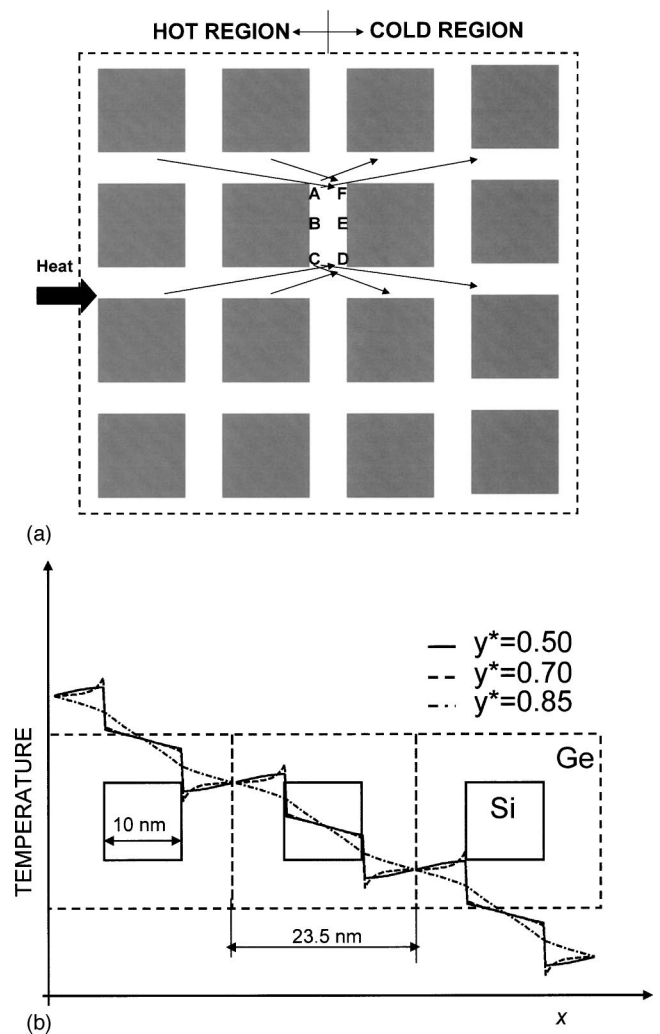


FIG. 4. (a) Illustration to show the mechanisms of negative temperature gradient in the localized regions using thermal radiation analogy. (b) The temperature distribution along x^* at $y^*=0.5, 0.7,$ and 0.85 for $L_{Si}=10$ nm over three periods.

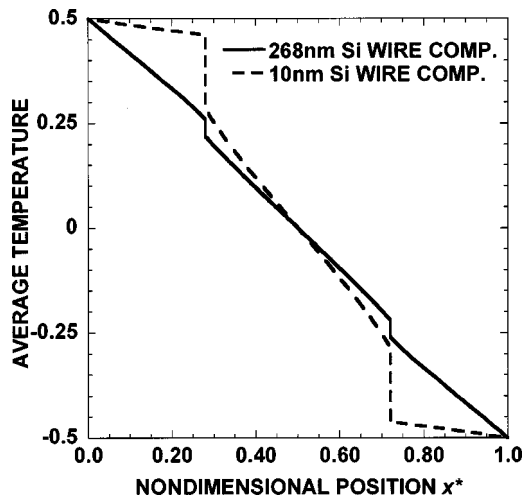


FIG. 5. The dimensionless average temperature distribution along the x direction in $\text{Si}_{0.2}\text{-Ge}_{0.8}$ composite with silicon wire dimension of $L_{\text{Si}} = 268$ nm and $L_{\text{Si}} = 10$ nm, respectively.

in-plane interface scattering is equivalent to a fraction of $(L_{\text{Ge}} - L_{\text{Si}})/L_{\text{Ge}}$ cross-interface scattering. In other words, the efficiency of cross-interface scattering to reduce thermal conductivity is around five times as effective as the scattering parallel to the interface. This result is consistent with previous experiments and modeling of the in-plane and cross-plane thermal conductivity of superlattices.^{14,16} It also suggests that the anisotropic nanocomposites might be more effective in reducing thermal conductivity of nanocomposites.

IV. CONCLUSIONS

We studied theoretically the phonon thermal conductivity of periodic two-dimensional nanocomposites with nanowires

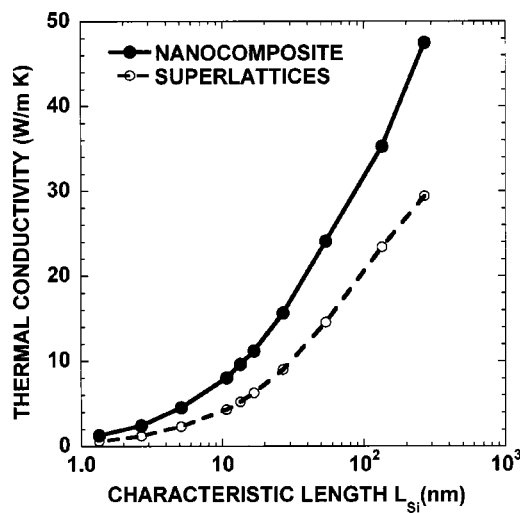


FIG. 6. Thermal conductivity of $\text{Si}_{0.2}\text{-Ge}_{0.8}$ composites as a function of the silicon wire dimension or layer thickness. The smaller the characteristic length of silicon (the silicon wire dimension in composites and the thickness of the silicon layer in superlattices), the smaller is the thermal conductivity.

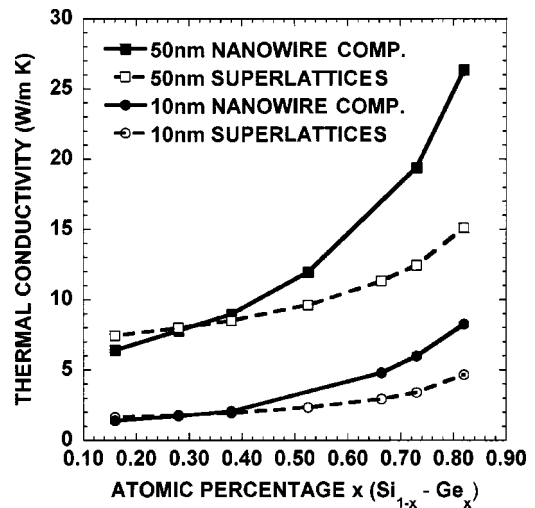


FIG. 7. Thermal conductivity of $\text{Si}_{1-x}\text{-Ge}_x$ composites as a function of atomic percentage x of germanium. For fixed silicon wire dimension, the lower the atomic percentage of germanium, the lower is the thermal conductivity of the nanocomposites. The result is very different from the bulk material due to the ballistic nature of phonon transport at nanoscale and interface effect.

embedded in a host semiconductor material using the phonon BE. Special attention has been paid to cell-cell interaction using periodic boundary conditions. The simulation shows that the temperature profiles in nanocomposites are very different from those in conventional composites due to ballistic phonon transport at nanoscale. Such temperature profiles cannot be captured by existing models in literature. We predict the thermal conductivity dependence on the interface conditions, the size of the nanowires, and the volumetric fraction of the constituent materials. The smaller the wire diameter, the smaller is the thermal conductivity of periodic two-dimensional nanocomposites. The thermal conductivity of 2D Si-Ge composites is predicted to be a function of the atomic percentage of germanium for wire dimensions of 50 and 10 nm. It shows that for fixed silicon wire dimension, the lower the atomic percentage of germanium, the lower the thermal conductivity of the

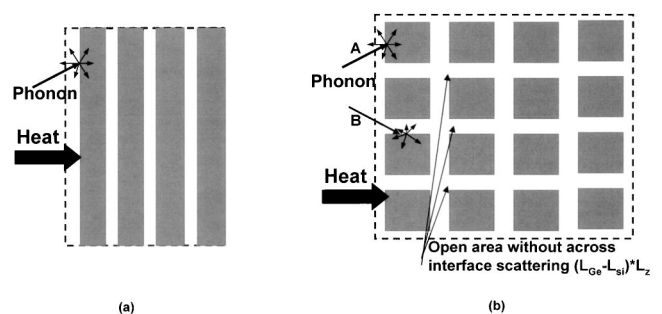


FIG. 8. Illustration to show that phonons experience less cross-interface scattering in periodic 2D composites than that in 1D layered structures but additional scattering parallel to the interface. The efficiency of cross-interface scattering to reduce thermal conductivity is around five times as effective as scattering parallel to the interface.

nanocomposites. This is very different from bulk composites because the interface dominates the ballistic transport in nanocomposites. The periodic 2D nanocomposites can have a lower thermal conductivity than their 1D counterpart when the Ge atomic percentage is lower than 35%. This suggests that the anisotropic nanocomposites might be more effective in reducing thermal conductivity of nanocomposites. Results of this study can be used to direct the development of both high efficiency thermoelectric materials and thermal inter-

face material with high thermal conductivity particle or wire inclusions.

ACKNOWLEDGMENTS

The authors would like to thank Professor M.S. Dresselhaus, W. L. Liu, and C. Dames for comments and useful discussions. R.Y. would like to acknowledge the help from Yong Li. The work was financially supported by DOE BES (DE-FG02-02ER45977) and NSF (CTS-0129088).

*Electronic address: gchen2@mit.edu

- ¹H. J. Golosmid, *Thermoelectric Refrigeration* (Plenum, New York, 1964).
- ²Special Issues on Thermoelectrics, edited by T. M. Tritt, *Semicond. Semimetals* **69–71** (2001).
- ³M. S. Dresselhaus, Y. M. Lin, S. B. Cronin, O. Rabin, M. R. Black, G. Dresselhaus, and T. Koga, *Semicond. Semimetals* **71**, 1 (2001).
- ⁴G. Chen, *Semicond. Semimetals* **71**, 2003 (2001).
- ⁵R. Venkatasubramanian, *Semicond. Semimetals* **71**, 175 (2001).
- ⁶T. C. Harman, P. J. Taylor, M. P. Walsh, and B. E. LaForge, *Science* **297**, 2229 (2002).
- ⁷R. Venkatasubramanian, E. Silvana, T. Colpitts, and B. O'Quinn, *Nature (London)* **413**, 597 (2001).
- ⁸G. Chen, D. Borca-Tasciuc, and R. G. Yang, in *Encyclopedia of Nanoscience and Nanotechnology*, edited by H. S. Nalwa (American Scientific Publishers, Stevenson Ranch, CA, 2004), Vol. 7, N68.
- ⁹B. Yang and G. Chen, *Phys. Rev. B* **67**, 195311 (2003).
- ¹⁰P. Hyldgaard and G. D. Mahan, *Phys. Rev. B* **56**, 10754 (1997).
- ¹¹S. Tamura, Y. Tanaka, and H. J. Maris, *Phys. Rev. B* **60**, 2627 (1999).
- ¹²W. E. Bies, R. J. Radtke, and H. Ehrenreich, *J. Appl. Phys.* **88**, 1498 (2000).
- ¹³B. Yang and G. Chen, *Microscale Thermophys. Eng.* **5**, 107 (2001).
- ¹⁴G. Chen, *ASME J. Heat Transfer* **119**, 220 (1997).
- ¹⁵G. Chen and M. Neagu, *Appl. Phys. Lett.* **71**, 2761 (1997).
- ¹⁶G. Chen, *Phys. Rev. B* **57**, 14958 (1998).
- ¹⁷P. Hyldgaard and G. D. Mahan, *Therm. Conduct.* **23**, 172 (1996).
- ¹⁸M. V. Simkin and G. D. Mahan, *Phys. Rev. Lett.* **84**, 927 (2000).
- ¹⁹B. Daly, H. Maris, K. Imamura, and S. Tamura, *Phys. Rev. B* **66**, 024301 (2002).
- ²⁰C. Dames and G. Chen, *J. Appl. Phys.* **95**, 682 (2004).
- ²¹G. W. Milton, *The Theory of Composites* (Cambridge University Press, New York, 2002).
- ²²P. L. Kapitza, *J. Phys.* **4**, 181 (1941); for a review on thermal boundary resistance, see Ref. 49.
- ²³D. P. H. Hasselman and L. F. Johnson, *J. Compos. Mater.* **21**, 508 (1987).
- ²⁴Y. Benvensite, *J. Appl. Phys.* **61**, 2840 (1987); Y. Benvensite and T. Miloh, *ibid.* **69**, 1337 (1991).
- ²⁵A. G. Every, Y. Tzou, D. P. H. Hasselman, and R. Raj, *Acta Metall. Mater.* **40**, 123 (1992).
- ²⁶C.-W. Nan, R. Birringer, D. R. Clarke, and H. Gleiter, *J. Appl. Phys.* **81**, 6692 (1997).
- ²⁷C.-W. Nan and F. S. Jin, *Phys. Rev. B* **48**, 8578 (1993); C.-W. Nan, *J. Appl. Phys.* **76**, 1155 (1994).
- ²⁸P. A. Smith and S. Torquato, *J. Appl. Phys.* **65**, 893 (1989); S. Torquato and M. D. Rintoul, *Phys. Rev. Lett.* **75**, 4067 (1995).
- ²⁹R. Lipton and B. Vernescu, *J. Appl. Phys.* **79**, 8964 (1996).
- ³⁰See, for example, M. Jiang, I. Jasiuk, and M. Ostojca-Starzewski, *Comput. Mater. Sci.* **25**, 329 (2002); F. W. Jones and F. Pascal, *Geophysics* **60**, 1038 (1995).
- ³¹S. Graham and D. L. McDowell, *ASME J. Heat Transfer* **125**, 389 (2003).
- ³²K. Ramani and A. Vaidyanathan, *J. Compos. Mater.* **29**, 1725 (1995).
- ³³M. R. Islam and A. Pramila, *J. Compos. Mater.* **33**, 1699 (1999).
- ³⁴A. Khitun, A. Balandini, J. L. Liu, and K. L. Wang, *J. Appl. Phys.* **88**, 696 (2000); *Superlattices Microstruct.* **30**, 1 (2001); A. Khitun, K. L. Wang, and G. Chen, *Nanotechnology* **11**, 327 (2000); J. L. Liu *et al.*, *Phys. Rev. B* **67**, 165333 (2003).
- ³⁵O. L. Lazarenkova and A. A. Balandin, *J. Appl. Phys.* **89**, 5509 (2001); *Phys. Rev. B* **66**, 245319 (2002); A. A. Balandin and O. L. Lazarenkova, *Appl. Phys. Lett.* **82**, 415 (2003).
- ³⁶J. M. Ziman, *Electrons and Phonons* (Oxford University Press, London, 1985).
- ³⁷R. Prasher, *Appl. Phys. Lett.* **83**, 48 (2003); *ASME J. Heat Transfer* **125**, 1156 (2003).
- ³⁸A. Majumdar, *ASME J. Heat Transfer* **115**, 7 (1993).
- ³⁹G. Chen and C. L. Tien, *J. Thermophys. Heat Transfer* **7**, 311 (1993).
- ⁴⁰R. Siegel and J. R. Howell, *Thermal Radiation Heat Transfer*, 4th ed. (Taylor & Francis, Washington, D.C., 2001).
- ⁴¹M. F. Modest, *Radiative Heat Transfer*, 2nd ed. (Academic Press, New York, 2003).
- ⁴²A. A. Joshi and A. Majumdar, *J. Appl. Phys.* **74**, 31 (1993).
- ⁴³P. G. Klemens, *Solid State Phys.* **7**, 1 (1958).
- ⁴⁴K. E. Goodson and Y. S. Ju, *Annu. Rev. Mater. Sci.* **29**, 261 (1999).
- ⁴⁵P. Markowich, C. Ringhofer, and C. Schmeiser, *Semiconductor Equations* (Springer, Wien, 1990).
- ⁴⁶R. G. Yang, G. Chen, M. Laroche, and Y. Taur, *ASME J. Heat Transfer* (to be published).
- ⁴⁷R. M. Costescu, M. A. Wall, and D. G. Cahill, *Phys. Rev. B* **67**, 054302 (2003).
- ⁴⁸D. G. Cahill, W. K. Ford, K. E. Goodson, G. D. Mahan, A. Majumdar, H. J. Maris, R. Merlin, and S. R. Phillpot, *J. Appl. Phys.* **93**, 793 (2003).
- ⁴⁹E. T. Swartz and R. O. Pohl, *Rev. Mod. Phys.* **61**, 605 (1989).
- ⁵⁰W. A. Fiveland, *ASME J. Heat Transfer* **109**, 809 (1987); J. S. Truelove, *ibid.* **109**, 1048 (1987).
- ⁵¹G. D. Raithby, *Numer. Heat Transfer, Part B* **35**, 389 (1994).